Exploring the Sensitivity of Water Temperature Models for High Dams and Large Reservoirs: A Case Study of the Nuozhadu Reservoir in China

Lejun Ma [1,2,3], Changjun Qi [4,*], Chengyuan Zhao [5] and Yufeng Jiang [3,6]

1   College of Hydrology and Water Resources, Hohai University, Nanjing 210098, China; ljma@jit.edu.cn
2   School of Network Security, Jinling Institute of Technology, Nanjing 211169, China
3   Henan Key Laboratory of Water Environment Simulation and Treatment, Zhengzhou 450001, China; jyfhhu@njit.edu.cn
4   Appraisal Center for Environment and Engineering, The Ministry of Ecology and Environment of China, Beijing 100012, China
5   Huaneng Lancang River Hydropower Inc., Kunming 650214, China; riverbasin@126.com
6   Nanjing Institute of Technology School of Civil Engineering and Architecture, Nanjing 211167, China
*   Correspondence: qcj882@126.com

Abstract: The parameters governing a water temperature model play a pivotal role in determining the uncertainties associated with the model's outcome. In this study, a two-dimensional (2D) hydrodynamic and water temperature coupling model is constructed, focusing on the Nuozhadu Reservoir situated along the Lancang River. Employing a single-factor analysis approach, the sensitivity of the thermal balance parameters and hydrodynamic parameters in the model is assessed. This study overcomes the shortcomings of previous sensitivity analyses of hydrodynamic parameters in reservoir water temperature models. The findings reveal that the attenuation parameters of light and Beer's law parameter exhibit minimal sensitivity to the vertical temperature structure. Conversely, radiation parameter A and radiation parameter B exert tenfold disparate influences on the surface and bottom temperatures of the reservoir. Among the hydrodynamic parameters considered, the horizontal viscosity factor shows no sensitivity to the vertical temperature structure, whereas the vertical viscosity factor serves as a crucial determinant, directly influencing the intensity of vertical temperature stratification. An increased vertical viscosity factor promotes heat exchange between the upper and lower water layers, thereby reducing the vertical temperature gradient and weakening stratification. Conversely, diminishing this factor intensifies stratification. Thus, when conducting water temperature simulations in high dams and large reservoirs, careful attention should be given to calibrating vertical viscosity factor.

Keywords: high dams and large reservoirs; parameter sensitivity analysis; water temperature model; vertical temperature structure

1. Introduction

The construction and operation of high dams and large reservoirs play pivotal roles in providing energy support for social and economic development, while also serving as crucial engineering safeguards for the optimal allocation of water resources. However, importantly, these factors also significantly impact the temporal and spatial distributions of water temperature within a reservoir's water body and the downstream river section below the dam. Research shows that the construction of dams damages the connectivity of rivers and blocks fish migration channels, thus affecting aquatic biodiversity [1,2]. Simultaneously, reservoir storage changes the natural hydrological situation in the river channel, reducing the flow rate in the downstream river section [3,4]. High dams and large reservoirs can also cause vertical temperature stratification in reservoir areas, make the bottom water temperature of the reservoir significantly lower than the natural river water temperature,

and result in a low-temperature water discharge phenomenon [5,6]. For example, the bottom water temperature of Fengmang Reservoir in Jilin Province, China, is approximately 4.0 °C [7,8], that of Longyangxia Reservoir in Qinghai Province is approximately 6.0 °C [9], that of Xin'anjiang Reservoir in Zhejiang Province is approximately 10 °C [10,11], that of Ertan Dam in Sichuan Province is approximately 10–11.5 °C [12], that of Guangzhou Zhuoluo Dam in Guizhou Province is approximately 16 °C [13], that of Nuozhadu Dam in Yunnan Province is approximately 17 °C [14,15], and that of Songtao Dam in Hainan Province is approximately 19 °C [16,17].

The stratification of water temperature in reservoirs and the consequent discharge of frigid water have crucial ecological impacts stemming from the establishment of large dams and reservoirs. To comprehensively grasp the ecological significance of these structures and strategize sound conservation measures, it is imperative to investigate the spatiotemporal distribution patterns of water temperature across reservoir regions. This constitutes a paramount research focus for hydroelectric projects of notable importance. Researchers have employed the Delft3D model as a two-dimensional simulation model for surface water temperature to identify the mechanisms and trends of climate change alongside reservoir operation policies that impact the water temperature in large reservoirs [18]. In another study, several researchers developed an ISM-RWTS model and documented the water temperature in the Tankeng Reservoir area, Zhejiang Province, China, achieving high precision and accuracy [19]. Similarly, a two-dimensional water temperature model was constructed to scrutinize the vertical distribution of the surface water temperature in Nuozhadu Reservoir [20]. Compared with empirical formulas for reservoir water temperature prediction, numerical models can generally obtain better simulation results [21].

To attain better simulation outcomes, calibration and the optimization of water temperature model parameters are fundamental steps that researchers extensively employ. Importantly, the uncertainty of model parameters strongly influences the uncertainty of water temperature model simulation results. For this reason, sensitivity analyses and assessments of the parameters in water temperature models are crucial for parameter calibration and have immense practical significance for performing accurate reservoir water temperature simulations [22,23].

The parameters of different reservoir water temperature models are not the same but can generally be divided into two categories: heat balance parameters and hydrodynamic parameters. Heat balance parameters directly impact the heat exchange process between reservoirs and the external environment; notable examples include solar absorption parameters, radiation parameters, and evaporation parameters [24–26]. On the other hand, hydrodynamic parameters mainly include riverbed slope, roughness, momentum exchange parameters, and vortex viscosity. Scholars worldwide have analyzed reservoir water temperature model parameters. Regrettably, few studies have been conducted on the sensitivity of water temperature model parameters for high dams and large reservoirs [27,28].

Nuozhadu Reservoir is the largest hydropower project on the Lancang River, with a total installed capacity of 5.85 million kilowatts and a core rockfill dam with a height of 261.5 m; this structure is among the largest dams in the world [29]. The reservoir is a multiyear regulation reservoir with a normal storage level of 812.0 m and a total storage capacity of 23.703 billion m^3. The backwater length of the main stream of the reservoir is approximately 215 km, and the average river width in the reservoir area is approximately 690 m; this type of reservoir is a typical channel-type high-dam reservoir (Figure 1).

This study aims to explore the relationship between various parameters in a water temperature model and simulate the reservoir water temperature in high dams and large reservoirs. To achieve these objectives, the Nuozhadu Reservoir is selected as the research object, and a two-dimensional (2D) hydrodynamic–temperature coupling model is constructed. Different from previous studies, this paper fully considers the coupled characteristics of the flow field and temperature field in high dams and large reservoirs [30–32], and sensitivity studies of thermal equilibrium parameters and hydrodynamic parameters are conducted. Furthermore, in addition to studying thermal balance parameters, sensitiv-

ity analyses of the horizontal viscosity factor and vertical viscosity factor are conducted to further improve the reservoir water temperature model. The findings of our study provide a basis for improving the accuracy of water temperature simulations of high dams and large reservoirs and provide basic technical support for decision making related to reservoir ecosystem protection.
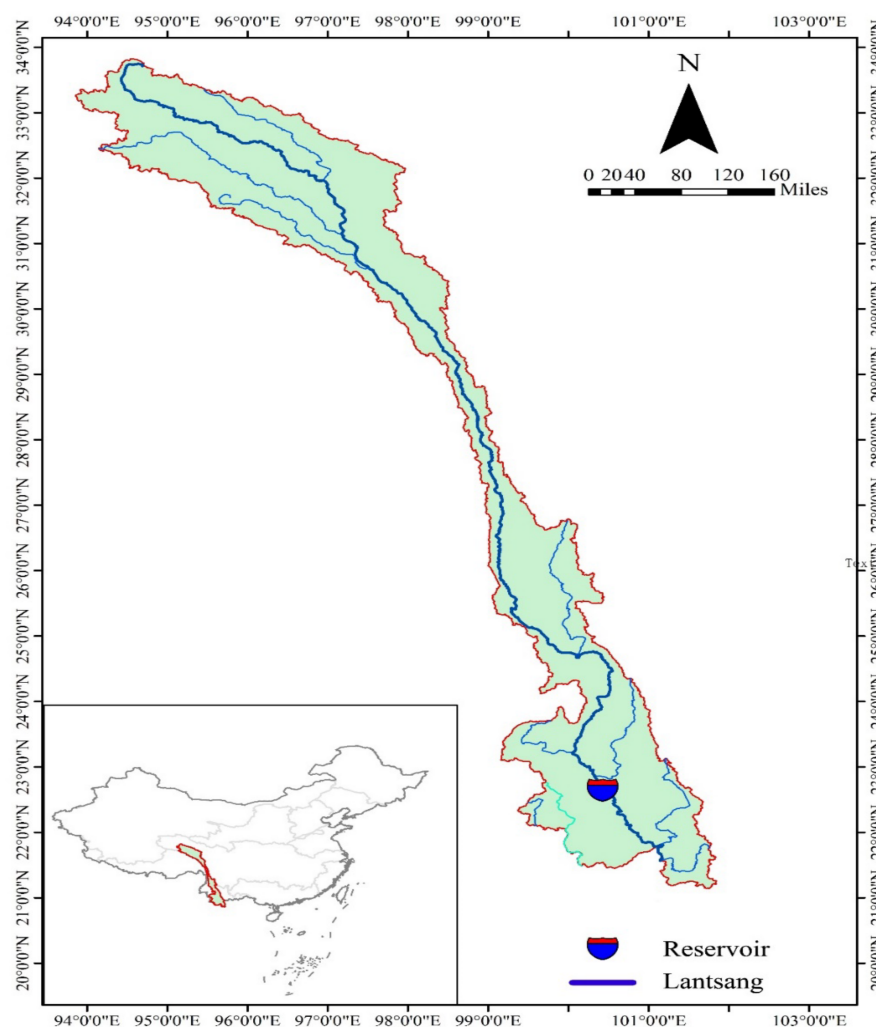

Figure 1. Location of the study area. The highlighted area in the image is within the Lancang River Basin, which is situated in southwestern China. The reservoir depicted in the image is Nuozhadu Reservoir on the Lantsang River.

2. Materials and Methods

Numerical water temperature models can be divided into one-dimensional, two-dimensional, and three-dimensional models according to their dimensions. Compared with one-dimensional models, two-dimensional models can fully reflect the water flow direction (vertical) and water depth direction (vertical) of a reservoir. Considering water temperature distribution characteristics, compared with 3D models of river-type reservoirs with limited lateral change in water temperature, 2D models are associated with fewer calculations and higher efficiency, while still meeting engineering design requirements [33–36].

2.1. Model Selection

The spatial distribution of hydrodynamic and water-quality factors in an actual channel is three dimensional, and simulations of channel flow characteristics can be based on two-dimensional or three-dimensional numerical models [37,38]. However, for river-type

reservoirs with hydrodynamic force, temperature, and concentration changes in the vertical direction that are much greater than those in the horizontal direction, a two-dimensional numerical model is sufficient [39,40]. For this reason, MIKE 11 software is used to construct a two-dimensional numerical model of the selected reservoir to study the distributions of the flow and temperature fields.

MIKE 11 is based on a finite difference scheme (the Abbott–Ionescu scheme), which is used to discretize the governing equations [41]. The basic equations of the hydrodynamic model are given as follows [42]:

$$\frac{\partial(Bu)}{\partial x} + \frac{\partial(Bw)}{\partial z} = Bq, \tag{1}$$

$$\frac{\partial(Bu)}{\partial t} + \frac{\partial(Bu^2)}{\partial x} + \frac{\partial(Bwu)}{\partial z} + \frac{B}{\rho}\frac{\partial P}{\partial x} = \frac{\partial}{\partial x}\left(BA_h\frac{\partial u}{\partial x}\right) + \frac{\partial}{\partial z}\left(BA_z\frac{\partial u}{\partial z}\right) - \frac{\tau_{wx}}{\rho}, \tag{2}$$

$$\frac{\partial P}{\partial z} + \rho g = 0, \tag{3}$$

where x denotes the longitudinal coordinate; z is the vertical coordinate; u and w are the longitudinal and vertical flow velocities (m/s), respectively; B represents the surface water width (m); A_h and A_z are the longitudinal and vertical eddy viscosity parameters, respectively (m^2/s); τ_{wx} denotes the sidewall resistance (N); q is the lateral inflow (s^{-1}); P is the pressure (Pa); ρ is the density of water (kg/m^3); and g is gravitational acceleration (m/s^2).

The basic equation of the water temperature model is given as follows:

$$\frac{\partial(BT)}{\partial t} + \frac{\partial(BuT)}{\partial x} + \frac{\partial(BwT)}{\partial z} = \frac{\partial}{\partial x}\left(BE_{tx}\frac{\partial T}{\partial x}\right) + \frac{\partial}{\partial z}\left(BE_{tz}\frac{\partial T}{\partial z}\right) + \frac{1}{\rho C_p}\frac{\partial(B\varphi)}{\partial z} + BqT_L \tag{4}$$

where T denotes the water temperature at altitude z at time t ($^\circ$C); E_{tx} and E_{tz} are the longitudinal and vertical diffusion parameters, respectively, for water temperature (m^2/s); T_L represents the temperature of source and sink terms ($^\circ$C); φ is the solar heat flux (Jm^{-2}s^{-1}); and C_p is the specific heat of water (Jkg^{-1} $^\circ$C^{-1}).

The turbulence model applied in this study is the widely used k$-\varepsilon$ turbulence model [43,44].

2.2. Model Building

In this paper, inflow, outflow, and water level data collected at Nuozhadu Reservoir were used to establish the hydrological boundary conditions of the model. In addition, the measured temperature, relative humidity, sunshine hours, wind speed, and wind direction data at the dam site were used to establish meteorological boundary conditions for the model. Using a 215 km water temperature model from the dam site to the tail of the reservoir, the water temperature distribution in Nuozhadu Reservoir was simulated for one year.

To ensure the reliability of the model, the vertical water temperature data collected at Nuozhadu Reservoir in 2014 were used to verify the model results (Figure 2). Our model accurately simulated the temporal evolution of the vertical water temperature near the dam throughout the year. Specifically, it aptly captured the emergence of a single thermocline in June and July, followed by a bifurcation into a double thermocline in August, September, and October. The region below 660 m is the hysteresis layer, which remains between 16.39 $^\circ$C and 17.30 $^\circ$C for the entire year.
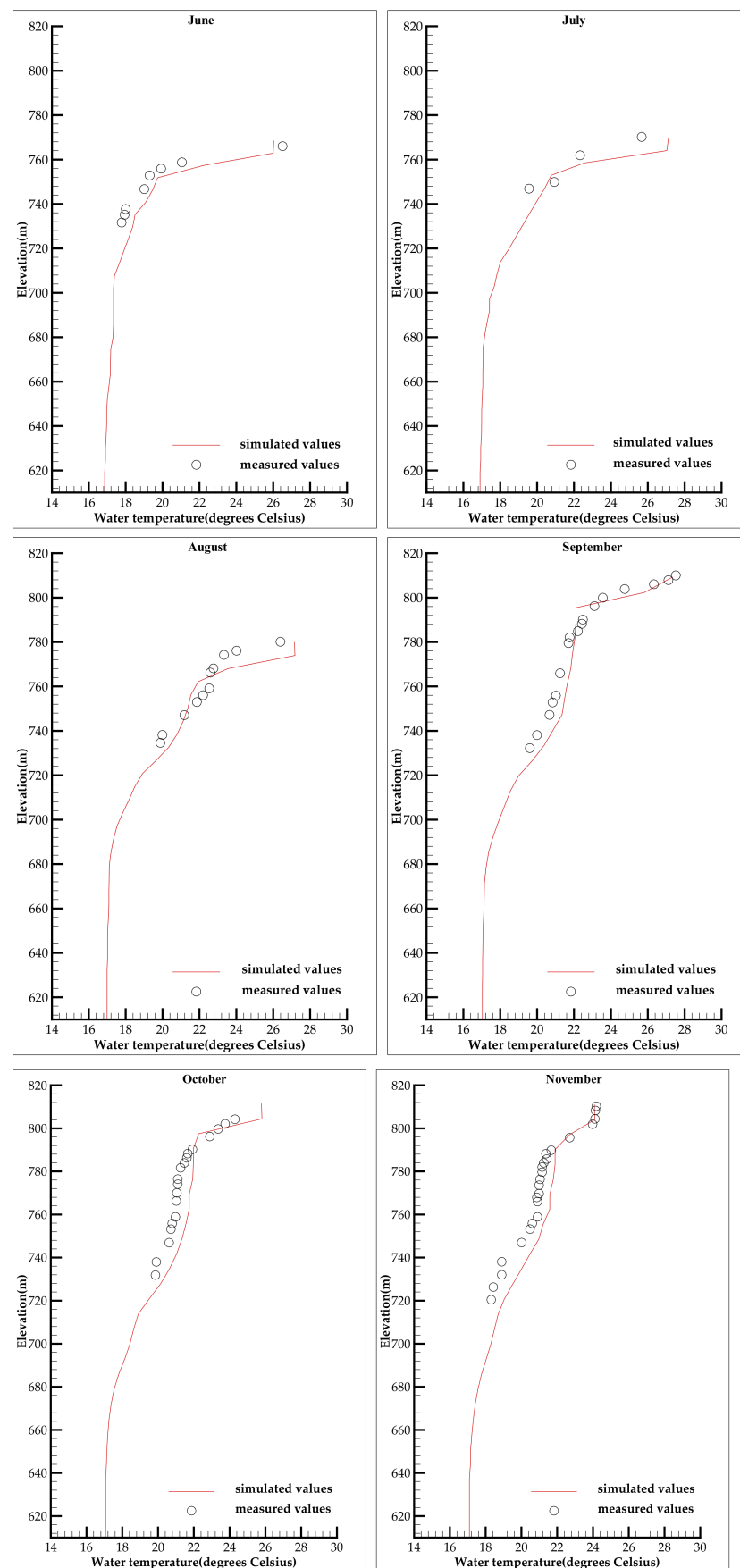
Figure 2. Comparison of the measured and simulated vertical water temperature structures.

2.3. Model Parameters

This paper focuses on sensitivity research on light attenuation and radiation parameters, heat balance parameters, and hydrodynamic parameters, such as the horizontal viscosity factor and vertical viscosity factor (Table 1). The initial values are the default values provided in MIKE11.

Table 1. Main parameters and values of the model.

Category	Name	Meaning	Unit	Initial Value	Updated Value
Basic parameters	Time step	Adaptive time step limit	Min	30	5
	Vertical layering	Vertically stratified body	Layer	10	30
	Light attenuation factor	Attenuation of solar radiation as it passes through a body of water	1/m	10	0.75
Heat balance parameters	Beer's law factor	The distribution of solar radiation in each layer of a water body	-	0	0.55
	Radiation parameter A	Intensity of solar radiation passing through clouds	-	0.2	0. 12
	Radiation parameter B		-	0.5	0.48
	Evaporation a	The heat loss when water body evaporation is closely related to the difference in vapor density between the surface water and the air, as well as the wind speed	-	1	1
	Evaporation b		-	1	1
	Manning value	A measure of the riverbed's resistance to water flow	$m^{1/3}/s$	30	30
Hydrodynamic parameters	Eddy viscosity factor	For turbulence model calculations	m^2/s	0.003	0.003
	Horizontal viscosity factor	Used to control horizontal and vertical diffusion in mass transport equations	-	1	0.1
	Vertical viscosity factor		-	1	0.4

Usually, air temperature is the main driver of water temperature changes [45–47]. In terms of scale, water temperature has a certain correlation with air temperature [48]. To avoid air temperature fluctuations that may lead to deviations in reservoir water temperature simulation results [49], a unified air temperature boundary is adopted for each parameter simulation scheme in this paper.

2.3.1. Heat Balance Parameters

1.   Light attenuation parameters

The light attenuation parameter expresses the attenuation of solar radiation in water and is calculated as follows based on Beer's law formula:

$$E_{fac} = I_0(1 - \beta)\exp(-\alpha(D - z)), \tag{5}$$

where E_{fac} is the solar radiation intensity at water depth $(D - z)$, I_0 is the light intensity below the surface water, and $D - z$ is the distance from the water surface to different layers.

There are two parameters, α and β, in Beer's law formula. α is the light attenuation parameter, which reflects the attenuation of solar radiation in water, and the general value range is 0.5~1.4. β is Beer's law factor (a constant in Beer's law), which indicates the absorption of solar radiation by surface water, and the value range is generally less than 1.

2.   Radiation parameters

Radiation parameters are used to calculate the amount of radiation reaching the water surface during cloudy weather conditions, and the corresponding formula is given as follows:

$$E_{fac} = I_0(1 - \beta)\exp(-\alpha(D - z)), \tag{6}$$

$$A = 0.1 + 0.24 \left(\frac{\overline{n}}{\overline{N_d}} \right), \tag{7}$$

$$B = 0.38 + 0.08 \left(\frac{\overline{N_d}}{\overline{n}} \right), \tag{8}$$

H is the daily radiation amount under cloudy conditions, H_0 is the intensity of short-wave radiation in the atmosphere, n is the number of sunshine hours, and N_d is the length of a day and is based on the annual average values of n and N_d.

A and B are functions of sunshine hours and day length, called radiation parameter A and radiation parameter B, respectively; these parameters are used to describe the actual intensity of radiation passing through clouds. Usually, the range of A is 0.1~0.34, and the value of B is greater than 0.46.

3. Evaporation parameters

Evaporation parameters are used to calculate the evaporation heat loss of a water body, which is calculated based on Dalton's law and the Friehe and Smidth derivation formula:

$$q_e = LC_e(a + bW_2)(Q_w - Q_a), \tag{9}$$

where q_e is the heat loss caused by evaporation; L is the latent heat parameter of evaporation, which is 2.5×106 J/kg; C_e is the humidity factor, which is 1.32×10^{-3}; W_2 is the wind speed 2 m above the water surface; Q_w is the wind speed considering the near-surface water vapor density; and Q_a is the water vapor density in the air.

a and b are evaporation factors, where a reflects the degree of evaporation heat loss and b reflects the influence of wind speed on evaporation heat loss. This model does not consider the effect of evaporation, and a sensitivity analysis of the evaporation factor is not carried out. Here, $a = b = 1$.

2.3.2. Hydrodynamic Parameters

Hydrodynamic parameters play a crucial role in conducting sensitivity analyses of horizontal and vertical viscosity factors. The horizontal viscosity factor and vertical viscosity factor in the material transport equation help regulate horizontal and vertical diffusion processes. These factors are multiplied by the turbulent viscosity to obtain the horizontal and vertical diffusion in the transport equations. Specifically, the multiplication of the eddy viscosity factor and turbulent viscosity factor reflects the mixing of substances in water bodies and aids in accurately modeling flow dynamics.

2.4. Sensitivity Assessment and Analysis

One-way analysis of variance (ANOVA) was used to compare the means of two or more groups. ANOVA is not only simple, but also a powerful and robust method that provides more than just intuitive results. The method considers the variability in data between and within different groups, helping researchers determine whether the differences are significant.

In this study, we employed single-factor analysis to investigate the variations in the vertical water temperature structure near a dam by scrutinizing single parameters. To screen out highly sensitive parameters, we explored four value schemes for the light attenuation factor, Beer's law factor, radiation parameter A, radiation parameter B, the horizontal viscosity factor, and the vertical viscosity factor. Analysis Scenario 2 served as the benchmark for investigating the impacts of distinct parameter values on the simulation results (refer to Table 2). Notably, option 2 includes the calibrated model value and serves as the reference condition for the parameter sensitivity analysis.
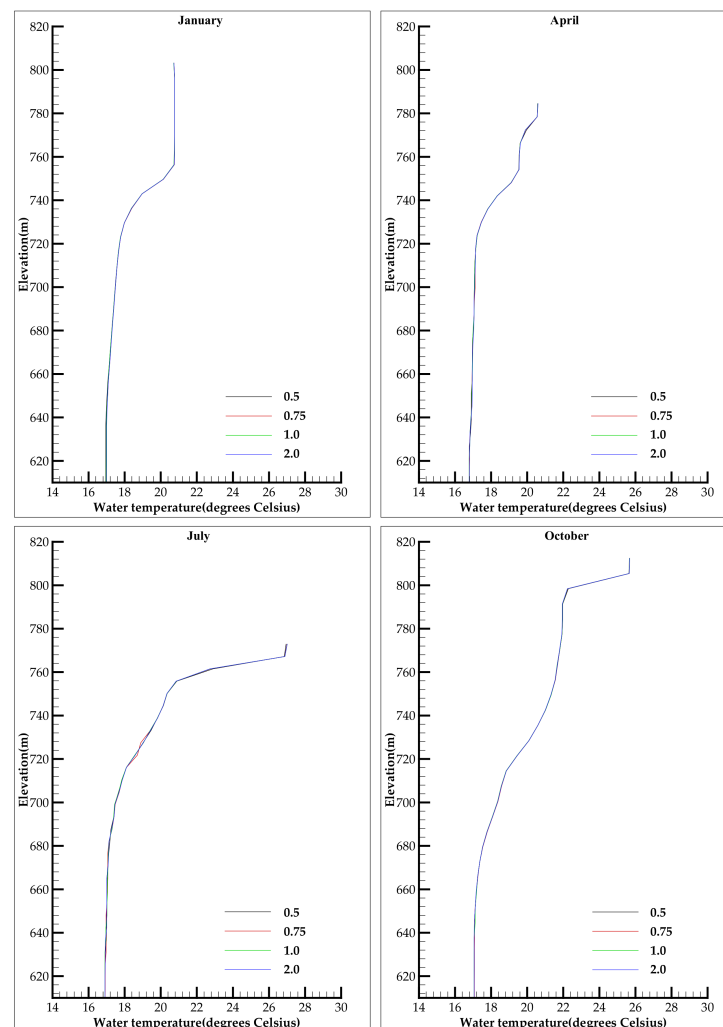
Table 2. The value of each parameter.

Parameters	Value	Analysis Scenario 1	Analysis Scenario 2 (Benchmark)	Analysis Scenario 3	Analysis Scenario 4
Light attenuation parameter		0.5	0.75	1.0	2.0
Beer's parameter		0.1	0.55	0.8	1.0
Radiation parameter A		0.1	0.12	0.15	0.34
Radiation parameter B		0.46	0.48	0.55	0.8
Horizontal viscosity factor		0	0.1	0.5	1.0
Vertical viscosity factor		0	0.4	0.8	1.0

Moreover, considering the seasonal variations in water temperature, based on the above schemes, the changes in the vertical water temperature structure of each scheme in January, April, July, and September are analyzed, and the sensitivity of each parameter to the vertical water temperature structure is assessed (Table 2).

3. Results

3.1. Light Attenuation Parameter

Figure 3 shows the simulated water temperature and the actual water temperature structure for different values of water temperature when the light attenuation parameter is 0.5, 0.75 (benchmark scheme), 1.0, and 2.0.

Figure 3. Vertical water temperature distribution for different light attenuation parameters.

The results of Plan 1, Plan 3, Plan 4, and the benchmark scheme are basically the same. The maximum difference in the surface water temperature of the reservoir each month is 0.05, the maximum difference in the water temperature at the bottom of the reservoir is 0.04 °C, and the maximum difference in the average water temperature is 0.01 °C. This result suggests that the light attenuation parameter is not sensitive to the structure of the water temperature.

3.2. Beer's Law Parameter

The different Beer's law parameter values indicate a decreasing water temperature with depth, as shown in Figure 4. The results obtained for Plans 1, 2, 3, and 4 are basically the same. The maximum difference in the surface water temperature of the reservoir each month is 0.04 °C, the maximum difference in water temperature at the bottom of the reservoir is 0.04 °C, and the maximum difference in the average water temperature is 0.01 °C. This result suggests that the Beer's law parameter has no obvious impact on the calculation results. Thus, this parameter is a nonsensitive parameter.
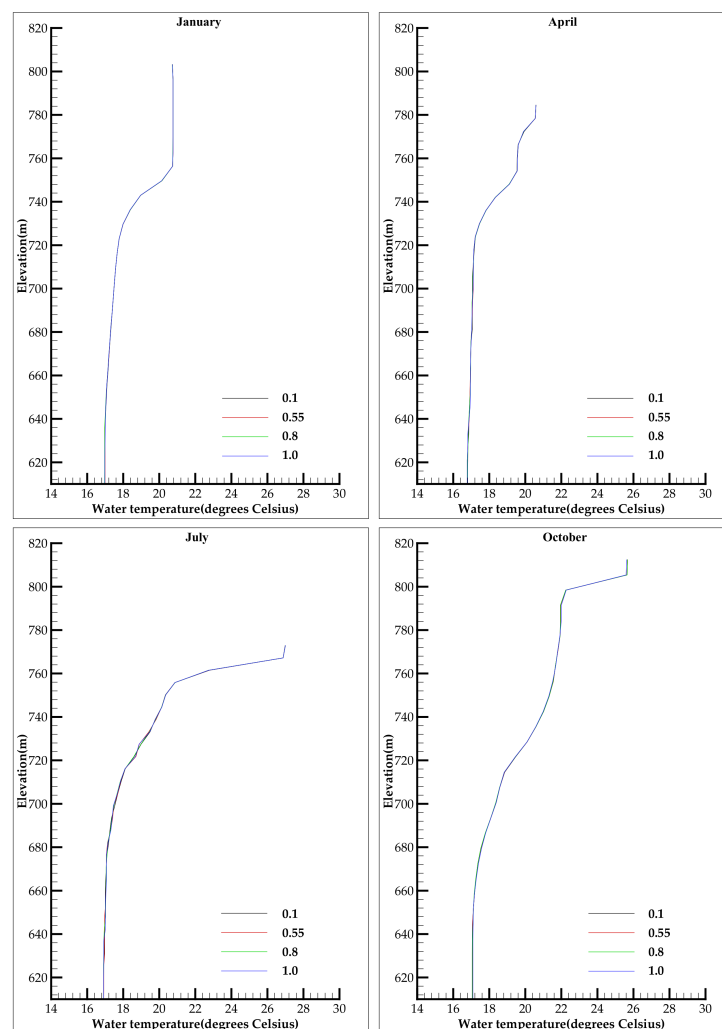

Figure 4. Vertical water temperature distribution with different Beer's law parameter values.

3.3. Radiation Parameter A

Figure 5 shows the water temperature structure diagram for different radiation parameters. The results indicate that the different radiation parameter A values result in differences in the surface water temperature, the deep-layer water temperature, and the average water temperature of the reservoir.
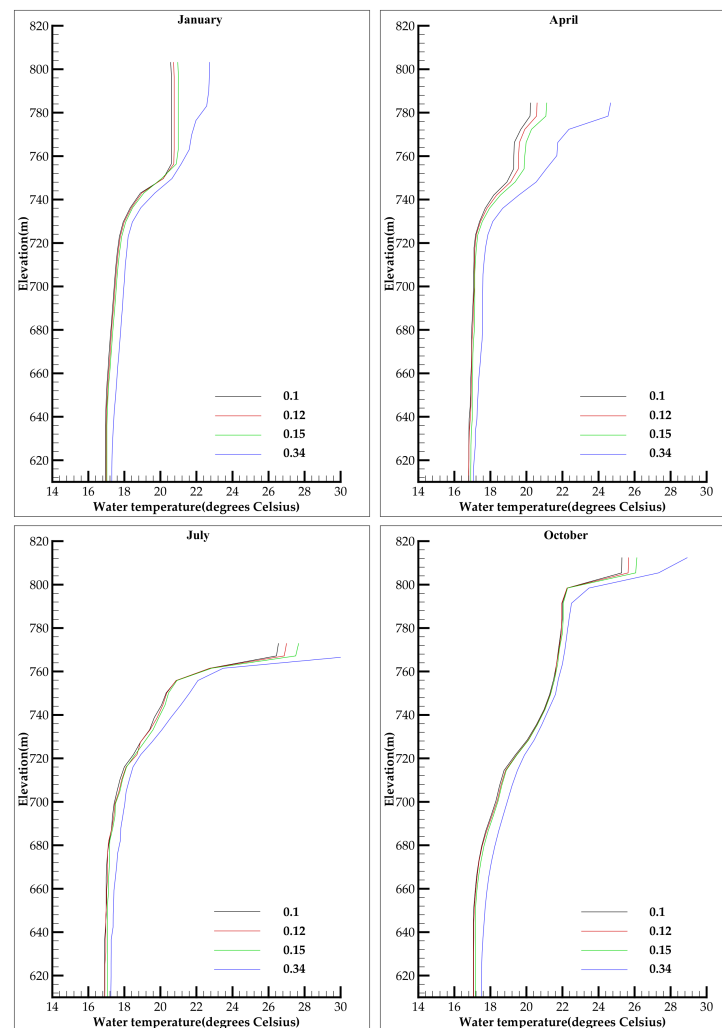
Figure 5. Vertical water temperature distribution with different values of radiation parameter A.

When radiation parameter A is 0.1, the surface water temperature, deep-layer water temperature, and average water temperature of the reservoir each month are less than those in the benchmark scheme (0.12), and the maximum differences are 0.45 °C, 0.05 °C, and 0.09 °C, respectively. When radiation parameter A is 0.15, the surface water temperature, deep-layer water temperature, and average water temperature of the reservoir each month are greater than those in the benchmark scheme (0.12), and the maximum differences are 0.67 °C, 0.14 °C, and 0.16 °C, respectively. When radiation parameter A is 0.34, the surface water temperature, deep-layer water temperature, and average water temperature of the reservoir during each month are greater than those in the benchmark scheme (0.12), and the maximum differences are 4.69 °C, 0.57 °C, and 0.98 °C, respectively.

Furthermore, there is a difference in the influence of radiation parameter A on the temperature of the surface water and the deep-layer water. Compared with the calculated results of 0.1 and 0.34, the maximum difference in the surface water temperature each month is 5.14 °C, and the minimum difference is 2.15 °C; additionally, the maximum difference in the water temperature at the bottom layer each month is 0.59 °C, and the minimum difference is 0.23 °C. Radiation parameter A is sensitive to the surface water temperature of the reservoir and is relatively insensitive to the impact of the bottom water temperature of the reservoir.

3.4. Radiation Parameter B

The surface water temperature, deep-layer water temperature, and average water temperature of the reservoir are shown for each month.

Different values of radiation parameter B yield different changes in the calculated water temperatures. Notably, the surface water temperature, deep-layer water temperature, and average water temperature of the reservoir are different among the schemes (Figure 6).
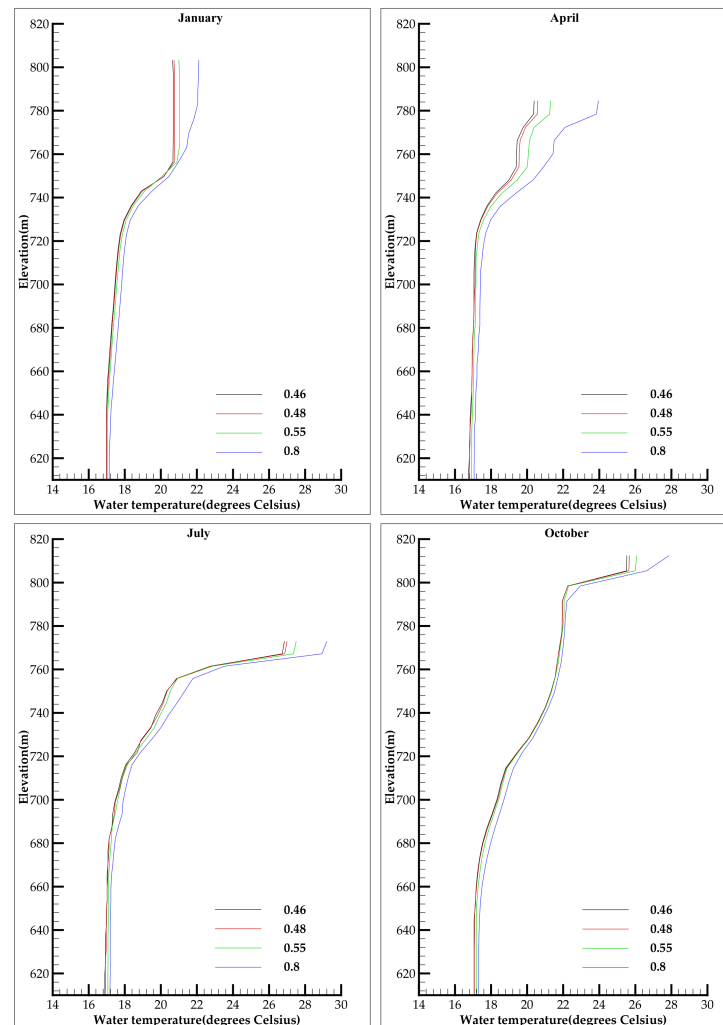

Figure 6. Vertical water temperature distribution with different values of radiation parameter B.

When radiation parameter B is 0.46, the surface water temperature, deep-layer water temperature, and average water temperature of the reservoir each month are less than those in the benchmark scheme, and the maximum differences are 0.24 °C, 0.03 °C, and 0.05 °C, respectively.

When radiation parameter B is 0.55, the surface water temperature, deep-layer water temperature, and average water temperature of the reservoir each month are greater than those in the benchmark scheme, and the maximum differences are 0.8 °C, 0.16 °C, and 0.2 °C, respectively.

When radiation parameter B is 0.8, the surface water temperature, deep-layer water temperature, and average water temperature of the reservoir each month are greater than those in the benchmark scheme, and the maximum differences are 3.64 °C, 0.32 °C, and 0.79 °C, respectively.

In summary, radiation parameter B is a sensitive parameter that has a more significant influence on surface water temperature than on bottom water temperature.

3.5. Horizontal Viscosity Factor

The water temperature structures obtained for different horizontal viscosity factors are shown in Figure 7. A comparison of the calculated values of the water temperature for Analysis Scenario 3 and Plan 4 reveals that the maximum difference in the surface water temperature of the reservoir each month is 0.19 °C, the maximum difference in the water temperature at the bottom of the reservoir is 0.04 °C, and the maximum difference in the average water temperature is 0.03 °C. This result suggests that different schemes have no obvious impact on the results of the water temperature calculation, and that the reservoir is not sensitive to changes in the horizontal viscosity factor.
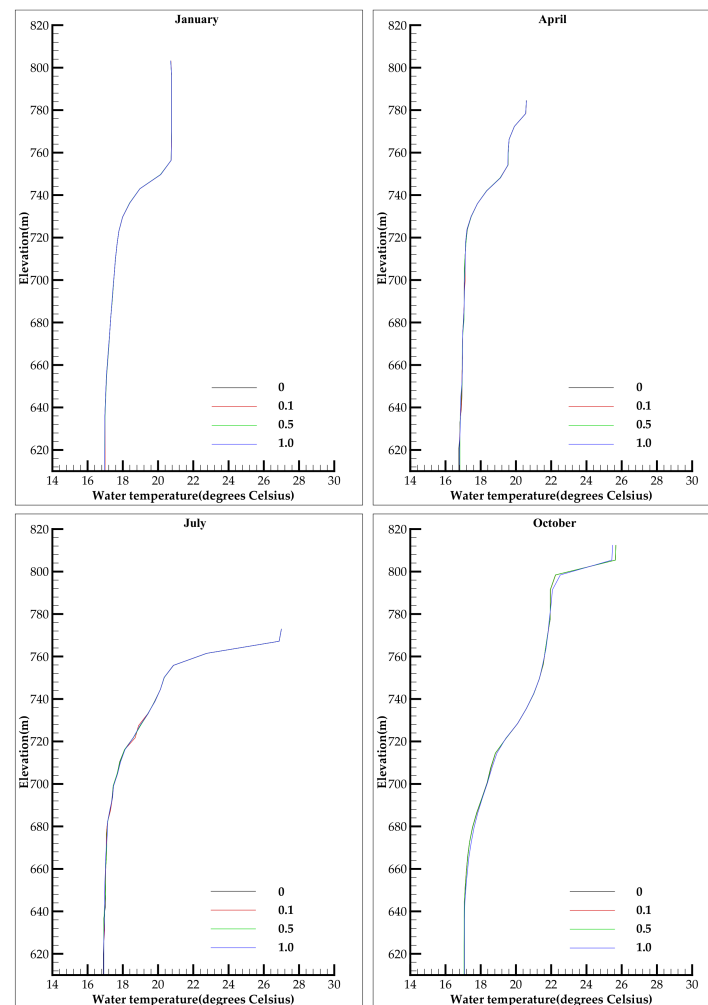

Figure 7. Vertical water temperature distribution for different horizontal viscosity factors.

3.6. Vertical Viscosity Factor

The effects of the vertical viscosity factor on the water temperature in different schemes are shown in Figure 8. The water temperature distribution changes when the vertical viscosity factor varies. The surface water temperature, deep-layer water temperature, and average water temperature are significantly different from those in the reference case. The corresponding data analysis results are as follows:

(1) The values in Analysis Scenario 1 are less than the benchmark scheme values. When the vertical viscosity factor is set to 0, the surface water temperature each month is greater than that in the benchmark scheme (0.4), with a maximum difference of 1.58 °C, and the deep-layer water temperature is less than that in the benchmark scheme (0.4), with a maximum difference of 1.29 °C. Additionally, the average water temperature each month is less than the average water temperature in the benchmark scheme (0.4), and the maximum

difference is 0.76 °C. Figure 8 shows that when the vertical viscosity factor is 0, the change in water temperature per month is highest in the deep layer.

(2) The values in Analysis Scenario 3 are greater than those in the benchmark scheme. When the vertical viscosity factor is 0.8, the surface water temperature each month is less than that in the benchmark scheme (0.4), and the maximum difference is 0.43 °C. The deep-layer water temperature is greater than that in the benchmark scheme (0.4), and the maximum difference is 0.69 °C. The average water temperature each month is greater than that in the benchmark scheme (0.4), and the maximum difference is 0.39 °C. Figure 8 shows that when the vertical viscosity factor increases, the vertical stratification of water temperature becomes weakened.

(3) In Analysis Scenario 4, as the vertical viscosity factor further increases, the vertical stratification of water temperature further weakens (Figure 8). For example, when the vertical viscosity factor is 1.0, the surface water temperature each month is less than that in the benchmark scheme (0.4), and the maximum difference is 0.56 °C. The maximum difference in the deep-layer water temperature is 0.79 °C. The average water temperature each month is greater than that in the benchmark scheme (0.4), with a maximum difference of 0.45 °C.

A comparison of the calculated values of water temperature when the vertical viscosity factor is 0 and 1.0 reveals that the maximum difference in surface water temperature each month is 2.0 °C, and the minimum difference is 0.19 °C. Additionally, the maximum difference in water temperature at the bottom of the reservoir is 2.05 °C, and the minimum difference is 0.94 °C. Unlike radiation parameters A and B, the vertical viscosity factor has an obvious influence on the surface and bottom water temperatures of the reservoir and is sensitive to the vertical water temperature structure.
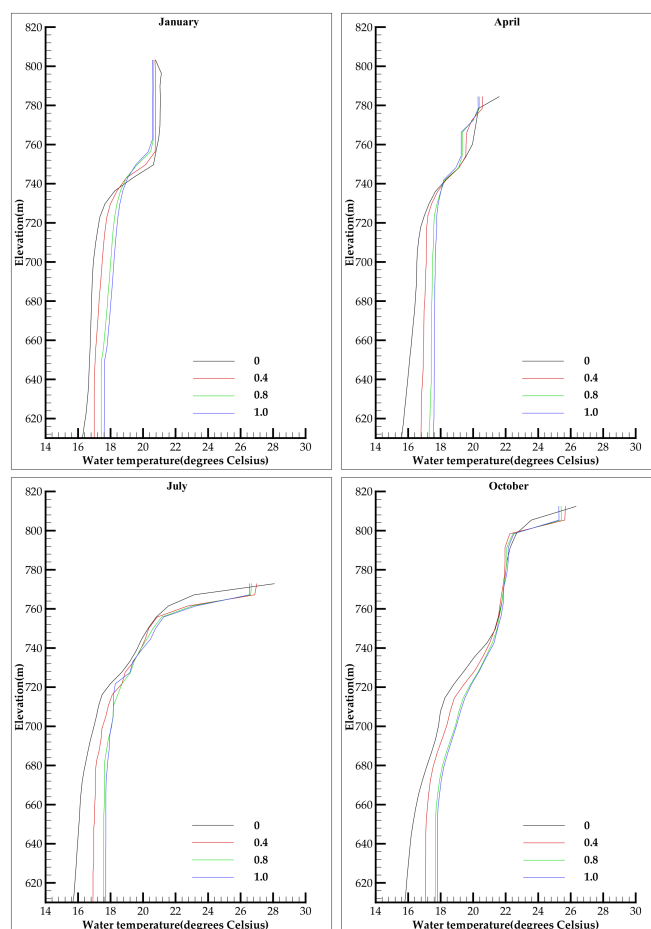

Figure 8. Vertical water temperature distribution for different vertical viscosity factors.

4. Discussion

Heat balance parameters: The transfer of heat across the reservoir surface is directly influenced by solar radiation and is highly sensitive to the temperature of the water at the reservoir surface. In the case of deep and large reservoirs, such as Nuozhadu Reservoir, the transmission of solar radiation to the lower reaches of the water body leads to the continuous loss of heat. The little heat that can be transmitted to the lower strata of the reservoir is offset by weak convection and diffusion. As a result, the temperature in the lower layers of the reservoir remains relatively low throughout the year. Compounding this issue, the surface water temperature of the reservoir shifts in accordance with the air temperature, further exacerbating the vertical stratification of the reservoir water temperature.

This study demonstrated that variations in radiation parameters A and B have distinguishable impacts on the temperatures of surface water and bottom water, revealing differences in their extents of influence. The vertical water temperature structure is mainly impacted by radiation parameters in the upper water body. For instance, under scenarios in which radiation parameter A is set at 0.1 and 0.34, the maximum difference among the monthly surface water temperatures reaches 5.14 °C, with a maximum difference of 0.59 °C occurring at the bottom of the reservoir. Similarly, in scenarios in which radiation parameter B is set to 0.46 and 0.8, the maximum difference among the monthly surface water temperatures reaches 3.88 °C, with a maximum difference of 0.33 °C occurring at the bottom of the reservoir. In terms of numerical shifts, the impact of radiation parameters on surface water temperature versus bottom water temperature differs by approximately tenfold.

Hydrodynamic parameters: Compared to other parameters, the vertical viscosity factor is found to exert a unique influence on the vertical temperature structure of reservoirs. It directly modulates the strength of the vertical stratification of water temperature, which plays a critical role in shaping the temperature profile of aquatic ecosystems. Our investigation revealed that when the vertical viscosity factor increased, the heat exchange between the upper and lower water layers of the reservoir strengthened, and consequently, the vertical water temperature gradient decreased, leading to a weakened vertical stratification of the water temperature. Conversely, when the vertical viscosity factor decreased, heat transfer between different water layers was impeded, and the vertical water temperature gradient increased, further strengthening the layered structure of the reservoir. This phenomenon provides an essential basis for understanding the stable stratification of the vertical water temperature in high dams and large reservoirs. Therefore, we recommend that researchers conducting water temperature simulation studies prioritize investigating the impact of the vertical viscosity parameter.

5. Conclusions

In this paper, we constructed a two-dimensional (2D) hydrodynamic and water temperature coupling model to investigate the structure of Nuozhadu Reservoir and used measured water temperature data to verify the reliability of the model. We explored the relationships between various parameters and the water temperature of the reservoir. To achieve our research objective, we conducted an exhaustive analysis of the essential model parameters, including four heat balance parameters (namely, the coefficient of light attenuation, Beer's parameter, and radiation parameters A and B) and two hydrodynamic parameters (namely, horizontal viscosity factor and vertical viscosity factor). This detailed and methodical investigation serves to fill the gap in the sensitivity analyses of hydrodynamic parameters in prior studies of the sensitivity of reservoir water temperature model parameters. Furthermore, this study sheds new light on the significance of hydrodynamic attributes, which were frequently overlooked in prior investigations of sensitivity related to model parameters in the context of reservoir water temperature analysis. Based on our findings, we suggest that future researchers prioritize investigating the impact of these hydrodynamic factors to gain a comprehensive understanding of this complex phenomenon.

(1) Our study showed that the light attenuation factor and Beer's law parameter are not significant contributors to the vertical water temperature structure of Nuozhadu Reservoir. Radiation parameter A and radiation parameter B, on the other hand, display some influence on the reservoir surface water temperature, but their impact on the reservoir bottom water temperature is relatively limited. Moreover, their influence on the vertical water temperature structure is mainly observed in the upper part of the water body.

(2) Our analysis showed that the horizontal viscosity factor has little effect on the vertical water temperature structure. In contrast, the vertical viscosity factor is more sensitive than other parameters and has a crucial influence on the reservoir surface and bottom water temperatures. When the value of the vertical viscosity factor increases, the vertical stratification of the water temperature weakens, and vice versa.

(3) High dams and large reservoirs often exhibit vertical stratification in water temperature due to low solar radiation heat and weak convective diffusion in deeper water layers. This situation results in the existence of a hysteresis layer with a comparatively low water temperature throughout the year, further aggravating the vertical stratification of the reservoir water temperature.

Data Availability Statement: The datasets generated during and/or analyzed during the current study are not publicly available due to obligation to the data provider, but are available from the corresponding author on reasonable request.

Conflicts of Interest: Author Chengyuan Zhao was employed by Huaneng Lancang River Hydropower Inc. The remaining authors declare that the research was conducted in the absence of any commercial or financial relationships that could be construed as a potential conflict of interest.

References

1. Zhang, H.; Kang, M.; Shen, L.; Wu, J.; Li, J.; Du, H.; Wang, C.; Yang, H.; Zhou, Q.; Liu, Z.; et al. Rapid change in Yangtze fisheries and its implications for global freshwater ecosystem management. *Fish Fish.* **2020**, *21*, 601–620. [CrossRef]
2. Liu, X.; Qin, J.; Xu, Y.; Ouyang, S.; Wu, X. Biodiversity decline of fish assemblages after the impoundment of the Three Gorges Dam in the Yangtze River Basin, China. *Rev. Fish Biol. Fish.* **2019**, *29*, 177–195. [CrossRef]
3. Ma, L.; Wang, H.; Qi, C.; Zhang, X.; Zhang, H. Characteristics and Adaptability Assessment of Commonly Used Ecological Flow Methods in Water Storage and Hydropower Projects, the Case of Chinese River Basins. *Water* **2019**, *11*, 2035. [CrossRef]
4. Ma, L.; Zhang, X.; Wang, H.; Qi, C. Characteristics and Practices of Ecological Flow in Rivers with Flow Reductions Due to Water Storage and Hydropower Projects in China. *Water* **2018**, *10*, 1091. [CrossRef]
5. Michael, W.; Bertram, B.; Karsten, R. Minimizing environmental impact whilst securing drinking water quantity and quality demands from a reservoir. *River Res. Appl.* **2019**, *35*, 17–35.
6. Qi, C.; Lu, B. Study of the temporal and spatial distribution of water temperature in Ertan Reservoir based on prototype observation. *Adv. Mater. Res.* **2014**, *864–867*, 2278–2287. [CrossRef]
7. Zheng, T.; Sun, S.; Liu, H.; Jiang, H.; Li, G. Effect of the Elevation of Old Dam Gap on Water Temperature Discharged for Fengman Rebuilt Project. In Proceedings of the 2016 4th International Conference on Mechanical Materials and Manufacturing Engineering, Wuhan, China, 15–16 October 2016; pp. 372–375.
8. Tuo, Y.; Deng, Y.; Li, J.; Li, N.; Li, K.; Wei, L.; Zhao, Z. Effects of dam reconstruction on thermal-ice regime of Fengman Reservoir. *Cold Reg. Sci. Technol.* **2018**, *146*, 223–235. [CrossRef]
9. Quan, Q.; Wang, Y.; Shen, B. The Multi-Level Intake Structure of High-Altitude Reservoirs in Aquatic Environments. *J. Residuals Sci. Technol.* **2016**, *13*, 155–165.

10. Wang, F.; Maberly, S.C.; Wang, B.; Liang, X. Effects of dams on riverine biogeochemical cycling and ecology. *Inland Waters* **2018**, *8*, 130–140. [CrossRef]

11. Zhang, Y.; Wu, Z.; Liu, M.; He, J.; Shi, K.; Wang, M.; Yu, Z. Thermal structure and response to long-term climatic changes in Lake Qiandaohu, a deep subtropical reservoir in China. *Limnol. Oceanogr.* **2014**, *59*, 1193–1202. [CrossRef]

12. Lu, B.; Kang, Y.; Zhang, H.; Gu, H.; Jiang, S.; Hui, X.; Cao, Z.; Tung, Y.K. Field observation of water temperature profiles in large reservoirs with different features. In Proceedings of the 5th International Symposium on Integrated Water Resources Management, IWRM 2010 and the 3rd International Symposium on Methodology in Hydrology, Nanjing, China, 19–21 November 2010; IAHS-AISH Publication: Wallingford, UK, 2011; Volume 350, pp. 359–368.

13. Chen, D.; Chen, G.; Zhao, Z.; Xu, H.; Xia, H.; Guo, Y.; Fan, X. Guizhou Light Hydropower Station Die Liang Gate-level Water Effect Monitoring. *Environ. Impact Eval.* **2016**, *38*, 45–48+52.

14. Wang, F.; Ni, G.; Riley, W.J.; Tang, J.; Zhu, D.; Sun, T. Evaluation of the WRF lake module (v1.0) and its improvements at a deep reservoir. *Geosci. Model Dev.* **2019**, *12*, 2119–2138. [CrossRef]

15. Jiang, B.; Wang, F.; Ni, G. Heating Impact of a Tropical Reservoir on Downstream Water Temperature: A Case Study of the Jinghong Dam on the Lancang River. *Water* **2018**, *10*, 951. [CrossRef]

16. Gu, H.; Lu, B.; Qi, C.; Xiong, S.; Shen, W.; Ma, L. Water Temperature Simulation in a Tropical Lake in South China. *Water* **2021**, *13*, 913. [CrossRef]

17. Tan, S.; Zhou, W.; Huang, B.; Shi, J.; Deng, Y.; Tuo, Y. Study on water temperature stratification characteristics of reservoir in tropical region. *Yangtze River* **2019**, *50*, 65–70. (In Chinese) [CrossRef]

18. Wang, L.; Xu, B.; Zhang, C.; Fu, G.; Chen, X.; Zheng, Y.; Zhang, J. Surface water temperature prediction in large-deep reservoirs using a long short-term memory model. *Ecol. Indic.* **2022**, *134*, 108491. [CrossRef]

19. Yao, Y.; Gu, Z.; Li, Y.; Ding, H.; Wang, T. Intelligent Simulation of Water Temperature Stratification in the Reservoir. *Int. J. Environ. Res. Public Health* **2022**, *19*, 13588. [CrossRef] [PubMed]

20. Guo, S.; Zhu, D.; Chen, Y. Modelling and Analyzing a Unique Phenomenon of Surface Water Temperature Rise in a Tropical, Large, Riverine Reservoir. *Water Resour. Manag.* **2023**, *37*, 1711–1727. [CrossRef]

21. Qi, C.J.; Zhai, Y.; Lu, B.H.; Wang, Q.G. Research on Vertical Distribution of Water Temperature in Different Regulation Reservoirs. *Adv. Mater. Res.* **2014**, *955–959*, 3190–3197. [CrossRef]

22. Song, X.; Zhang, J.; Zhan, C.; Xuan, Y.; Ye, M.; Xu, C. Global sensitivity analysis in hydrological modeling: Review of concepts, methods, theoretical framework, and applications. *J. Hydrol.* **2015**, *523*, 739–757. [CrossRef]

23. Pianosi, F.; Beven, K.; Freer, J.; Hall, J.W.; Rougier, J.; Stephenson, D.B.; Wagener, T. Sensitivity analysis of environmental models: A systematic review with practical workflow. *Environ. Model. Softw.* **2016**, *79*, 214–232. [CrossRef]

24. Chen, C.; He, W.; Zhou, H.; Xue, Y.; Zhu, M. A comparative study among machine learning and numerical models for simulating groundwater dynamics in the Heihe River Basin, northwestern China. *Sci. Rep.* **2020**, *10*, 3904. [CrossRef] [PubMed]

25. Wang, Q.; Zhao, X.; Chen, K.; Liang, P.; Li, S. Sensitivity Analysis of Thermal Equilibrium Parameters of MIKE 11 Model: A Case Study of Wuxikou Reservoir in Jiangxi Province of China. *Chin. Geogr. Sci.* **2013**, *23*, 584–593. [CrossRef]

26. Chen, G.; Fang, X. Sensitivity Analysis of Flow and Temperature Distributions of Density Currents in a River-Reservoir System under Upstream Releases with Different Durations. *Water* **2015**, *7*, 6244–6268. [CrossRef]

27. Fan, S.; Feng, M.; Liu, Z. Simulation of water temperature distribution in Fenhe Reservoir. *Water Sci. Eng.* **2009**, *2*, 32–42.

28. Pekárová, P.; Miklánek, P.; Halmová, D.; Onderka, M.; Pekár, J.; Kučárová, K.; Liová, S.; Škoda, P. Long-term trend and multi-annual variability of water temperature in the pristine Bela River basin (Slovakia). *J. Hydrol.* **2011**, *400*, 333–340. [CrossRef]

29. Song, J.; Duan, X.; Han, X.; Li, Y.; Li, Y.; He, D. The accumulation and redistribution of heavy metals in the water-level fluctuation zone of the Nuozhadu Reservoir, Upper Mekong. *Caten* **2019**, *172*, 335–344. [CrossRef]

30. Chen, H.; Gao, X. Study on the hydraulic characteristics of multi-elevations intake of hydropower station. *J. Hydroelectr. Eng.* **2014**, *33*, 105–110. (In Chinese)

31. Fischer, H.; List, E.; Koh, R.; Imberger, J.; Brooks, N. *Mixing in Inland and Coastal Waters*; Academic Press: London, UK, 1979.

32. Wang, Y.; Politano, M.; Laughery, R. Towards full predictions of temperature dynamics in McNary Dam forebay using OpenFOAM. *Water Sci. Eng.* **2013**, *6*, 317–330.

33. Zhu, S.L.; Zhang, Z.L.; Liu, X.B. Enhanced Two Dimensional Hydrodynamic and Water Quality Model (CE-QUAL-W2) for Simulating Mercury Transport and Cycling in Water Bodies. *Water* **2017**, *9*, 643. [CrossRef]

34. Zhang, Z.; Sun, B.; Johnson, B. Integration of a benthic sediment diagenesis module into the two-dimensional hydrodynamic and water quality model—CE-QUAL-W2. *Ecol. Model.* **2015**, *297*, 213–231. [CrossRef]

35. Besma, Z.; Moncef, G. Two-dimensional modelling of hydrodynamics and water quality of a stratified dam reservoir in the southern side of the Mediterranean Sea. *Environ. Earth Sci.* **2014**, *72*, 3037–3051.

36. Wang, G.; Han, L.; Chang, W. Modeling water temperature distribution in reservoirs with 2D laterally averaged flow-temperature coupled model. *Water Resour. Prot.* **2009**, *25*, 59–63. (In Chinese)

37. ASCE Task Committee on Turbulence Models in Hydraulic Computations. Turbulent Modeling of Surface Water Flow and Transport: Part 1. *J. Hydraul. Eng.* **1988**, *114*, 971–991.

38. Van, R. Field verification of 2-D and 3-D suspended sediment models. *J. Hydraul. Eng.* **1990**, *116*, 1270–1288.

39. Falconer, R.; Owens, P. Numerical modelling of suspended sediment fluxes in estuarine waters. *Estuar. Coast. Shelf Sci.* **1990**, *31*, 745–762. [CrossRef]

40. Jiang, C.; Zhang, Q.; Gao, Z. A 2-D unsteady flow model for predicting temperature and pollutant distribution in vertical cross section of a river. *J. Hydraul. Eng.* **2000**, *9*, 20–24. (In Chinese) [CrossRef]
41. Abbott, M.B.; Ionescu, F. On The Numerical Computation of Nearly Horizontal Flows. *J. Hydraul. Res.* **1967**, *5*, 97–117. [CrossRef]
42. MIKE 11 Reference Manual Home Page. Available online: https://manuals.mikepoweredbydhi.help/2017/MIKE_11.htm (accessed on 1 December 2023).
43. Rodi, W. Examples of calculation methods for flow and mixing in stratified fluids. *J. Geophys. Res. Atmos.* **1987**, *92*, 5305–5328.
44. Shams Nia, H.; Hejazi, K. 2DV Nonlinear k-ε Turbulence Modeling of Stratified Flows. *J. Persian Gulf* **2012**, *3*, 7–16.
45. Caissie, D.; El-Jabi, N.; Satish, M.G. Modelling of maximum daily water temperatures in a small stream using air temperatures. *J. Hydrol.* **2001**, *251*, 14–28. [CrossRef]
46. Webb, B.; Clark, P.; Walling, D. Water-Air Temperature Relationships in A Devon River System and the Role of Flow. *Hydrol. Process.* **2003**, *17*, 3069–3084. [CrossRef]
47. Sahoo, G.; Schladow, S.; Reuter, J. Forecasting stream water temperature using regression analysis, artificial neural network, and chaotic non-linear dynamic models. *J. Hydrol.* **2009**, *378*, 325–342. [CrossRef]
48. Toffolon, M.; Piccolroaz, S. A hybrid model for river water temperature as a function of air temperature and discharge. *Environ. Res. Lett.* **2015**, *10*, 114011. [CrossRef]
49. Wang, Y.; Zhang, N.; Wang, D.; Wu, J. Impacts of cascade reservoirs on Yangtze River water temperature: Assessment and ecological implications. *J. Hydrol.* **2020**, *590*, 125240. [CrossRef]